Ultrafast exciton dynamics in one- and two-dimensional *para*-sexiphenyl clusters

Luxia Wang [*]

Department of Physics, University of Science and Technology Beijing, 100083 Beijing, China

Thomas Plehn[†] and Volkhard May [‡]

Institute of Physics, Humboldt-University at Berlin, Newtonstraße 15, D-12489 Berlin, Germany

Laser-pulse-induced ultrafast electronic excitation energy transfer in molecular systems is studied theoretically. As a particular excitation channel, we consider the simultaneous transition of different molecules into their first excited state. Accordingly, a restricted picture of the total nonlinear response of the molecular system on laser pulse excitation is obtained, but complete insight is gained on the contribution of the first excited states. To describe the temporal evolution of this multiexciton state, a direct computation of the related density matrix is circumvented. Instead, we derive equations of motion for expectation values of interest in using the quantum master equation governing the respective density operator. The subsequently generated hierarchy of kinetic equations is truncated following a general scheme. The whole approach is applied to a chain and a disk of *para*-sexiphenyl molecules. Different signatures of multiexciton effects are discussed.

I. INTRODUCTION

It is of ongoing interest to elucidate details of excitation energy transfer (EET) in dye aggregates, conjugated polymers, or supramolecular complexes [1]. A main reason for this research is the substantial importance of EET for the functionality of molecular-based optoelectronic devices and organic photovoltaic systems [2–5]. While EET in these examples is mainly a single-exciton phenomenon in a weakly excited system, also multiexciton effects, i.e., phenomena connected with the simultaneous excitation of many molecules, attract increasing attention. The most prominent example for such multiexciton effects represents the phenomenon of exciton-exciton annihilation (see recent work [6–13] and references therein). Another example of multiexciton effects has been described in Ref. [14] where the simultaneous excitation of different zinc-chlorine-type molecules into their first excited singlet state has been reported.

Interestingly, the theory of multiexciton phenomena in molecular systems is not of such a degree of elaboration as the description of respective processes in semiconductor nano-crystals and quantum dots (compare the representative work [15–18] from the last two decades on molecular systems with Ref. [19] focusing on solid state systems). Just the standard theory of Frenkel excitons has been improved recently (see, e.g., Refs. [20–22]). It is the aim of the present paper to continue work on multiexciton phenomena [23–29] (Refs. [26–29] focused on particular applications to plasmonic systems). Therefore, the approach on photoinduced multiexciton dynamics as suggested in Ref. [24] is embedded here in a generalized model of electronic excitations in a molecular system.

In the present paper, we ignore intramolecular electronic transitions to higher lying singlet states. The description is reduced to the excitation channel which only involves the simultaneous population of the first excited singlet state in different molecules. If the excitonic coupling is strong enough, this can be understood as the formation of many-exciton states (see Fig. 1).

Obviously, a restricted picture results of the total nonlinear response of the molecular system on laser-pulse-excitation. But we obtain a complete and clear view on the contribution of the first excited states. We consider such an approach as a reliable strategy. After investigating the formation of a many-exciton state, we will turn in a subsequent study to the inclusion of higher intermolecular electronic transitions. This will lead us directly to the consideration of what is known as exciton-exciton annihilation. Higher excited singlet states can be considered as suggested in Ref. [23]. Respective investigations represent work in progress.

The general description of multiexciton phenomena is applied to a chain and a disk formed by *para*-sexiphenyl (6P) molecules (see Figs. 2 and 3, respectively). We decided to take this type of molecule because of its large transition dipole moment of 12 D, resulting in a pronounced exciton splitting and also in subpicosecond EET. Moreover, as a part of a nanohybrid system, we already studied 6P molecules in a different respect (see Refs. [30–33]). We also emphasize that there are numerous experimental studies on 6P molecular systems (see, for example, Refs. [34–36] and references therein). The expected ultrafast EET is initiated by resonant laser-pulse excitation, which shall cover pulse durations from 20 fs to 1 ps.

[*]luxiawang@sas.ustb.edu.cn
[†]plehn@physik.hu-berlin.de
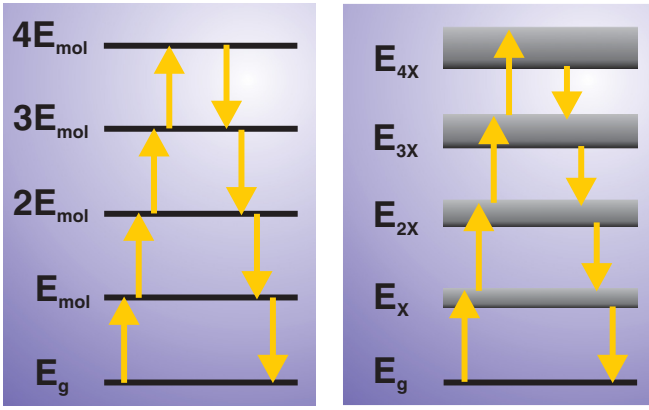[‡]may@physik.hu-berlin.de

FIG. 1. Nonlinear absorption and multiple excitation of the 6P molecular system (ground-state energy $E_g = 0$). Left panel: Multiple excitation NE_{mol} in the absence of EET coupling and electrostatic shifts. Right panel: Transitions among the multiexciton bands with energy E_{NX}.

The paper is organized as follows. The subsequent section introduces the model for the molecular system and Sec. III analyzes the hierarchy of kinetic equations. In Sec. IV, the general theory is applied to *para*-sexiphenyl systems. Some concluding remarks are presented in Sec. V. Details of the derivation may be found in the Supplemental Material (cf. Ref. [37]).

II. THE EXCITED STATE MODEL FOR THE MOLECULAR SYSTEM

To derive a model accounting for excited electronic states of molecules which form a cluster or aggregate, we follow the standard way (see, for example, Ref. [38]). It is complemented

by the consideration of electrostatic couplings among the different molecules. Higher excited molecular electronic states are part of the expansion but do not contribute in the spirit of polarization contributions (cf. Ref. [39]).

We start the derivation with an expansion of the whole molecular system Hamiltonian with respect to adiabatic single molecule electronic states φ_{ma}. Here, m counts the molecule and a labels the electronic level. Assuming molecular arrangements where intermolecular wave-function overlap is of minor importance or absent, we arrive at (cf. Ref. [38])

$$H_{mol} = \sum_{m,a} E_{ma} |\varphi_{ma}\rangle \langle \varphi_{ma}|$$
$$+ \frac{1}{2} \sum_{m,n} \sum_{a,b,c,d} J_{mn}(ab, cd) |\varphi_{ma}\rangle \langle \varphi_{mb}| \times |\varphi_{nc}\rangle \langle \varphi_{nd}|.$$
$$(1)$$

The given expression ignores nonadiabatic couplings, intramolecular vibrations, and refers to the ground-state nuclear configuration. The matrix elements of the intermolecular Coulomb coupling take the form

$$J_{mn}(ab, cd) = \langle \varphi_{ma} \varphi_{nc} | V_{mn} | \varphi_{nd} \varphi_{mb} \rangle$$
$$= \int d^3\mathbf{x} \, d^3\mathbf{y} \, \frac{n_{ab}^{(m)}(\mathbf{x}) n_{cd}^{(n)}(\mathbf{y})}{|\mathbf{x} - \mathbf{y}|}. \quad (2)$$

They are written in a way where a and b belong to molecule m and c and d to molecule n. The single-particle molecular charge densities read

$$n_{ab}^{(m)}(\mathbf{x}) = \rho_{ab}^{(m)}(\mathbf{x}) + \delta_{a,b} \sum_{\mu \in m} Q_\mu \delta(\mathbf{x} - \mathbf{R}_\mu). \quad (3)$$

The densities may also refer to the case $a \neq b$ due to the presence of the electronic transition charge density $\rho_{ab}^{(m)}$.
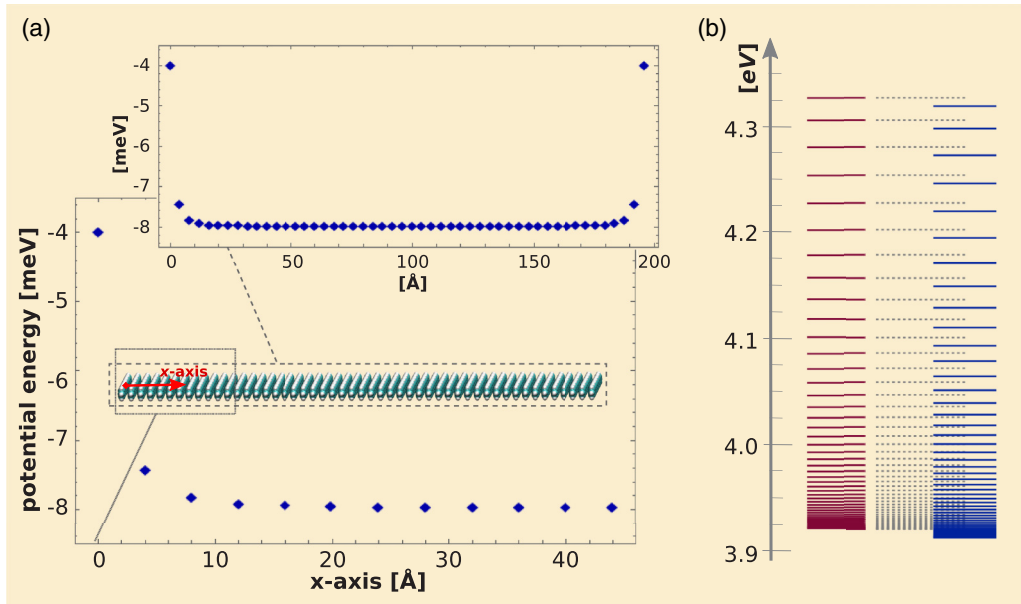

FIG. 2. 50 π-stacked 6P molecules forming a linear chain. (a) Relative electrostatic shift of the molecular excitation energies with respect to the gas-phase value of 4.02 eV (the lower left scheme enlarges the left edge area of the chain). (b) 6P Frenkel exciton band without (red) and with (blue) electrostatic shift of the molecular excitation energies.
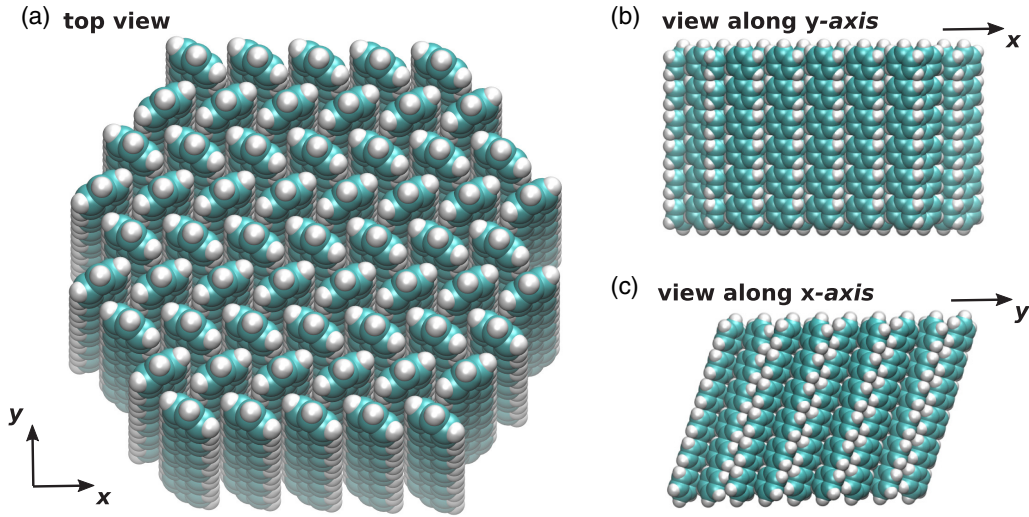
FIG. 3. Molecular disk formed by a monolayer of 59 6P molecules displaying a herringbone structure (top view and two side views are presented).

Moreover, μ counts the different nuclei which carry the effective charge Q_μ and belong to molecule m. A well-established approximation is given by the introduction of atomic-centered partial charges (transition charges) $q_{\mu ab}$ (cf. Ref. [32] and references therein):

$$n_{ab}^{(m)}(\mathbf{x}) = \sum_{\mu \in m} q_{\mu ab}\delta(\mathbf{x} - \mathbf{R}_\mu) \,. \qquad (4)$$

It results in the following Coulomb matrix element:

$$J_{mn}(ab, cd) \approx \sum_{\mu \in m}\sum_{\nu \in n} \frac{q_{\mu ab}q_{\nu cd}}{|\mathbf{R}_\mu - \mathbf{R}_\nu|}, \qquad (5)$$

which will also be used here. We remind the reader of the fact that this approach introduces EET coupling as an interaction far beyond any type of dipole-dipole coupling approximation.

A. Restriction to a two-electronic-level model

We restrict the description of the molecules to their ground state $|\varphi_{mg}\rangle$ and to their first excited state $|\varphi_{me}\rangle$. This enables us to formulate the whole Hamiltonian by means of a single type of molecular transition operator:

$$B_m^+ = |\varphi_{me}\rangle\langle\varphi_{mg}| \,. \qquad (6)$$

Note that $B_m B_m^+ = |\varphi_{mg}\rangle\langle\varphi_{mg}|$ and $B_m^+ B_m = |\varphi_{me}\rangle\langle\varphi_{me}|$ result in the completeness relation $1 = B_m B_m^+ + B_m^+ B_m$. Accordingly, we obtain the molecular Hamiltonian as

$$H_{\text{mol}} = \sum_m E_m B_m^+ B_m + \sum_{m,n} V_{mn} B_m^+ B_m B_n^+ B_n$$
$$+ \sum_{m,n}(J_{mn} B_m^+ B_n + \tilde{J}_{mn} B_m^+ B_n^+ + \tilde{J}_{mn}^* B_m B_n)$$
$$+ \sum_{m,n} \Delta J_{mn}(eg)B_m^+ B_m B_n^+ + \sum_{m,n} \Delta J_{mn}(ge)B_m^+ B_m B_n$$
$$+ \sum_{m,n}(J_{mn}(eg, gg)B_m^+ + J_{mn}(ge, gg)B_m). \qquad (7)$$

It generalizes the standard Hamiltonian (see, e.g., Ref. [38]) by different terms. The overall ground state is given by the product state,

$$|\phi_g\rangle = \prod_m |\varphi_{mg}\rangle, \qquad (8)$$

and the related ground-state energy is

$$E_g = \sum_m E_{mg} + \frac{1}{2}\sum_{m,n} J_{mn}(gg, gg). \qquad (9)$$

The expression includes the mutual Coulomb coupling of the individual molecules. For the following, it is suitable to set E_g equal to zero.

We explain the various ingredients of H_{mol}, Eq. (7), and start with the molecular excitation energy (site energy):

$$E_m = E_{me} - E_{mg} + \sum_n(J_{mn}(ee, gg) - J_{mn}(gg, gg)). \qquad (10)$$

The bare excitation energy $E_{me} - E_{mg}$ of molecule m is corrected by the Coulomb- coupling to all other molecules staying in their ground state. The second term of H_{mol} includes

$$V_{mn} = \tfrac{1}{2}(J_{mn}(gg, gg) - J_{mn}(ee, gg) - J_{mn}(gg, ee) + J_{mn}(ee, ee)). \qquad (11)$$

This combination of electrostatic shifts corrects the excitation energy if more than a single molecule is excited. We further introduced the EET (excitonic) coupling:

$$J_{mn} = J_{mn}(eg, ge). \qquad (12)$$

The additional terms,

$$\tilde{J}_{mn} = \tfrac{1}{2}J_{mn}(eg, eg), \qquad (13)$$

constitute the off-resonant part of the EET coupling. Finally, the quantities

$$\Delta J_{mn}(eg) = J_{mn}(ee, eg) - J_{mn}(gg, eg),$$
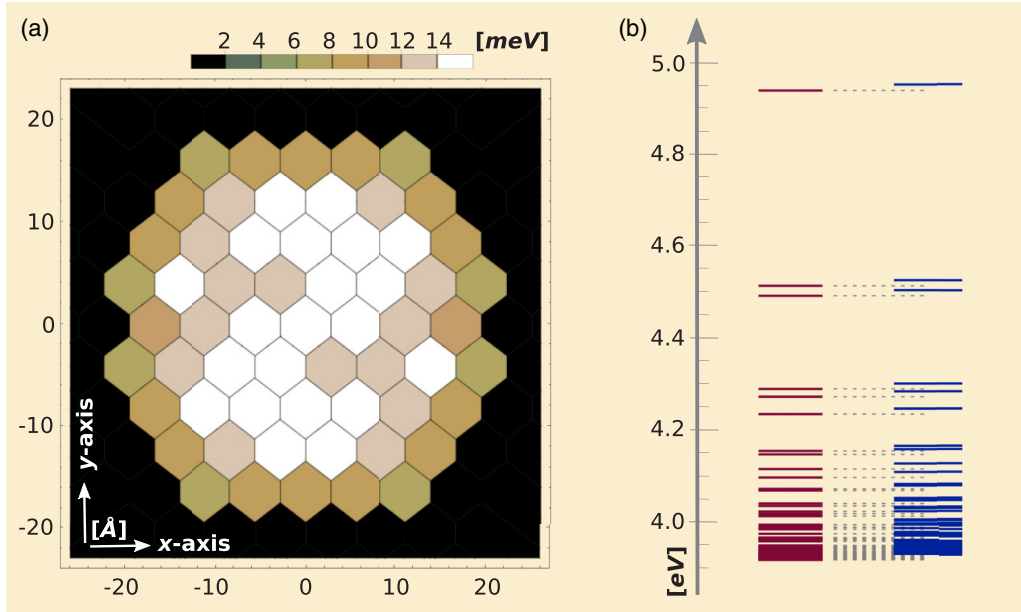$$\Delta J_{mn}(ge) = J_{mn}(ee, ge) - J_{mn}(gg, ge), \qquad (14)$$

FIG. 4. Fifty-nine 6P molecules forming a molecular disk. (a) Relative electrostatic shift of the molecular excitation energies with respect to the gas-phase value of 4.02 eV (color code see above). (b) 6P Frenkel exciton band without (red) and with (blue) electrostatic shift of the molecular excitation energies.

are originated by the coupling between ground-state or excited state densities and transition densities.

Noting the structure of H_{mol}, it is obvious that the terms proportional to $\tilde{J}$ and ΔJ as well as the last term in H_{mol}, Eq. (7), induce respective contributions in the kinetic equations which are all off resonant and can be neglected. Therefore, the Hamiltonian is reduced to

$$H_{\mathrm{mol}} = \sum_m \left(E_m + \sum_n V_{mn} B_n^+ B_n \right) B_m^+ B_m + \sum_{m,n} J_{mn} B_m^+ B_n,$$

$$(15)$$

but also extended by the coupling to a laser pulse:

$$H_{\mathrm{field}}(t) = -\mathbf{E}(t) \cdot \sum_m \mathbf{d}_m B_m^+ + \mathrm{H.c.}$$

$$\equiv \sum_m R_m(t) B_m^+ + \mathrm{H.c..} \qquad (16)$$

The electric-field strength,

$$\mathbf{E}(t) = \mathbf{n}_E E(t) e^{-i\omega_0 t} + \mathrm{c.c.,} \qquad (17)$$

refers to a single pulse with unit vector of field-polarization $\mathbf{n}_E$, with carrier frequency ω_0, and with pulse envelope

$$E(t) = E_0 \exp\left(-4\ln 2 \cdot (t - t_{\mathrm{p}})^2 / \tau_{\mathrm{p}}^2\right). \qquad (18)$$

We introduced the pulse-length τ_{p} as the full width at half maximum.

According to the above given extension, we may write the total Hamiltonian as

$$H(t) = H_{\mathrm{mol}} + H_{\mathrm{field}}(t). \qquad (19)$$

This Hamiltonian will be used to study multiexciton dynamics in 1D and 2D clusters of 6P molecules (see Figs. 2, 3, and 4, respectively). After the subsequent presentation of the general

kinetic theory of EET, we turn back to the two 6P systems and analyze their photoinduced dynamics.

III. HIERARCHY OF KINETIC EQUATIONS

A. Equations of motion for expectation values

To formulate a kinetic theory for photoexcited phenomena taking place in the considered set of two-level molecules, one can use the density-matrix theory. This would require to compute matrix elements of the reduced-density operator $\hat{\rho}(t)$ in using, for example, the multiple excited states:

$$|\psi_{N^*}\rangle = B_{m_1}^+ ... B_{m_{N^*}}^+ |\phi_g\rangle. \qquad (20)$$

These states correspond to $N^* < N_{\mathrm{mol}}$ molecules which are simultaneously placed in their singly excited electronic state. Then, the matrix elements of the density operator may refer to different numbers of excited molecules as well as to configurations which differ by the molecules which are in their excited state. Such an approach produces a huge number of density-matrix elements and, thus, it is restricted to a small number of molecules (in Ref. [26], we had to limit respective computations to less than ten molecules).

Therefore, it is more advantageous to directly compute expectation values like the molecular excited-state population:

$$P_m(t) = P_{me}(t) = \mathrm{tr}\{\hat{\rho}(t) B_m^+ B_m\} \equiv \langle B_m^+ B_m \rangle. \qquad (21)$$

When studying the photoinduced response of the molecular system, this quantity is of central interest. The ground-state population follows directly as

$$P_{mg}(t) = \mathrm{tr}\{\hat{\rho}(t) B_m B_m^+\} = 1 - P_m(t). \qquad (22)$$

We also introduce the ground-state excited-state transition amplitudes:

$$A_m(t) = \mathrm{tr}\{\hat{\rho}(t) B_m^+\} = \langle B_m^+ \rangle. \qquad (23)$$

Further types of single-molecule (single-site) functions do not exist. This is easily verified when introducing the general type of single-site function as $\mathrm{tr}\{\hat{\rho}(t)|\varphi_{ma}\rangle\langle\varphi_{mb}|\}$ (with $a, b = g, e$). For example, P_m is obtained for $a, b = e$ and A_m for $a = e$ and $b = g$.

To determine the introduced expectation values, related equations of motion have to be derived. Those are not closed but depend on other expectation values. In the case of $\langle B_m^+ B_m \rangle$, there appear $\langle B_m^+ \rangle$ and expressions like $\langle B_m^+ B_n \rangle$ $(m \neq n)$, and in the case of $\langle B_m^+ \rangle$ expressions like $\langle B_m^+ B_n^+ B_n \rangle$ are generated. This indicates that the whole approach establishes a hierarchy of equations. There, expectation values which refer to M different molecules are coupled to expectation values related to $M + 1$ molecules. An appropriate decoupling scheme has been suggested in Ref. [25] and is again explained briefly below.

We start with equations of motions for the different types of expectation values. They are deduced from the Markovian quantum master equation valid for the reduced-density operator:

$$\frac{\partial}{\partial t}\hat{\rho}(t) = -\frac{i}{\hbar}[H(t), \hat{\rho}(t)]_- - \mathcal{D}\hat{\rho}(t). \quad (24)$$

The unitary part is determined by the overall Hamiltonian $H(t)$, Eq. (19). The superoperator $\mathcal{D}$ is responsible for the actual type of dissipation. We consider dissipation due to molecular excited state decay [internal conversion (IC)], due to vibrational assisted EET among different molecules, and we account for pure dephasing of the ground-state excited-state transition.

For the present reasons, it is enough to derive $\mathcal{D}$ in the framework of the secular/second Born approximation, which results in a Lindblad-type variant of dissipation. This also offers an easy way to define the dissipative superoperator by means of the transition operators. Reference [37] gives a brief impression of the respective derivation, which starts from a microscopic model for the different processes.

Correspondingly, dissipation due to the decay of the excited molecular state with decay rate κ_m results in

$$-\mathcal{D}_{\mathrm{IC}}\hat{\rho}(t) = -\sum_m \frac{\kappa_m}{2}([B_m^+ B_m, \hat{\rho}(t)]_+ - 2B_m\hat{\rho}(t)B_m^+). \quad (25)$$

If vibrational-assisted EET from one molecule to another is considered, the dissipative superoperator reads

$$-\mathcal{D}_{\mathrm{EET}}\hat{\rho}(t) = -\sum_{m,n} \frac{k_{m\to n}}{2}([B_m^+ B_m B_n B_n^+, \hat{\rho}(t)]_+ - 2B_n^+ B_m\hat{\rho}(t)B_m^+ B_n). \quad (26)$$

The $k_{m\to n}$ denote the transition rates which will be specified later. Pure dephasing of the ground-state excited-state transition in a single molecule with rate $\gamma_m^{(\mathrm{pd})}$ leads to

$$-\mathcal{D}_{\mathrm{pd}}\hat{\rho}(t) = -\sum_m \gamma_m^{(\mathrm{pd})}(B_m^+ B_m\hat{\rho}(t)B_m B_m^+ + B_m B_m^+\hat{\rho}(t)B_m^+ B_m). \quad (27)$$

To derive equations of motion obeyed, for example, by the molecular excited-state population P_m, we consider the expec-

tation value of the arbitrary operator $\hat{O}$:

$$\langle \hat{O} \rangle = \mathrm{tr}\{\hat{\rho}(t)\hat{O}\}. \quad (28)$$

It is essential for the following that the respective equation of motion following from the quantum master equation can be rewritten to get a direct equation for $< \hat{O} >$:

$$\frac{\partial}{\partial t}\langle \hat{O} \rangle = \frac{i}{\hbar}\langle [H(t), \hat{O}]_- \rangle - \langle \tilde{\mathcal{D}}\hat{O} \rangle$$

$$= \left(\frac{\partial\langle \hat{O}\rangle}{\partial t}\right)_{\mathrm{coh}} + \left(\frac{\partial\langle \hat{O}\rangle}{\partial t}\right)_{\mathrm{diss}}. \quad (29)$$

The rearrangement of the original expression $\mathrm{tr}\{\partial\hat{\rho}(t)/\partial t \times \hat{O}\}$ first results in the commutator of $\hat{O}$ with the Hamiltonian. This is indicated as the coherent (unitary) part of the equation of motion. Second, the action of the dissipative superoperator on the density operator is changed to the action of a modified superoperator $\tilde{\mathcal{D}}$ on $\hat{O}$ and is indicated as the dissipative part of the equation of motion.

One easily derives the respective form of $\tilde{\mathcal{D}}$. For the case of dissipation due to IC, it results in

$$-\tilde{\mathcal{D}}_{\mathrm{IC}}\hat{O} = -\frac{1}{2}\sum_m \kappa_m([B_m^+ B_m, \hat{O}]_+ - 2B_m^+\hat{O}B_m). \quad (30)$$

In the case of dissipation due to vibrational assisted EET, we arrive at

$$-\tilde{\mathcal{D}}_{\mathrm{EET}}\hat{O} = -\frac{1}{2}\sum_{m,n} k_{m\to n}([B_m^+ B_m B_n B_n^+, \hat{O}]_+ - 2B_m^+ B_n\hat{O}B_n^+ B_m). \quad (31)$$

Finally, the process of pure dephasing leads to

$$-\tilde{\mathcal{D}}_{\mathrm{pd}}\hat{O} = -\sum_m \gamma_m^{(\mathrm{pd})}(B_m B_m^+\hat{O}B_m^+ B_m + B_m^+ B_m\hat{O}B_m B_m^+). \quad (32)$$

With Eq. (29) at hand, we can derive all necessary equations of motion. Their separation into a coherent and dissipative part has been introduced to become more flexible in the notation of the subsequent equations. Concerning the single-site functions, we have to compute equations of motion for $A_m = \langle B_m^+ \rangle$ and $P_m = \langle B_m^+ B_m \rangle$. They can be found in Ref. [37].

B. Two-site correlation function

The general form of two-site functions is given by

$$\hat{O}_{mn} = \mathrm{tr}\{\hat{\rho}(t)|\varphi_{ma}\rangle\langle\varphi_{mb}| \times |\varphi_{nc}\rangle\langle\varphi_{nd}|\}. \quad (33)$$

We have to distinguish between the expectation values $\langle B_k^+ B_m^+ B_m \rangle$, $\langle B_m^+ B_n \rangle$, $\langle B_m^+ B_n^+ \rangle$, and $\langle B_k^+ B_k B_m^+ B_m \rangle$. The first two functions appear in the equations of motion for the single-site functions. The function $\langle B_k^+ B_m^+ B_m \rangle$ correlates excitation of molecule k with the excited state population of molecule m. Excitation of molecule m is correlated with de-excitation of molecule n in $\langle B_m^+ B_n \rangle$. The correlation of the excitation of two different molecules is accounted for in $\langle B_m^+ B_n^+ \rangle$. It can be considered as a two-excitation (two-exciton) amplitude. Finally, the function $\langle B_k^+ B_k B_m^+ B_m \rangle$ considers correlation of the excited state population of molecule k and molecule m.

TABLE I. Parameters used.

N_{mol}	50, 59
E_{mol}	4.02 eV
d_{mol}	12.4 D
k	$10^{11}...10^{12}$/s
ω_0	varied around $E_{mol}/\hbar$
E_0	$10^6...10^8$ V/m
τ_p	20 fs... 2 ps

Equations of motion for all two-site functions are given in Ref. [37]. As it becomes obvious these equations contain different variants of three-site functions $\langle |\varphi_{ma}\rangle\langle\varphi_{mb}| \times |\varphi_{nc}\rangle\langle\varphi_{nd}| \times |\varphi_{ke}\rangle\langle\varphi_{kf}|\rangle$. In the next section, we offer an approximation scheme which removes the three-site functions. It is based on a general methodology to approximate higher-order correlations functions by lower order ones.

C. Decoupling scheme

To approximate N-site functions by lower order functions, we proceed according to Ref. [25] (see also Ref. [40]). Taking in a first step, the single-site operator $\hat{O}_m$, we introduce the

related operator of quantum fluctuations:

$$\Delta\hat{O}_m = \hat{O}_m - \langle\hat{O}_m\rangle. \tag{34}$$

Choosing $\hat{P}_n$ as another version of a single-site operator, the two-site correlation functions follow as

$$\langle\hat{O}_m\hat{P}_n\rangle = \langle\Delta\hat{O}_m\Delta\hat{P}_n\rangle + \langle\hat{O}_m\rangle\langle\hat{P}_n\rangle. \tag{35}$$

It splits into the so-called correlated part $<\Delta\hat{O}_m\Delta\hat{P}_n>$ and into the factorized part $<\hat{O}_m><\hat{P}_n>$. Introducing a third single-site operator $\hat{Q}_k$, the related three-site correlation function is expressed as

$$\begin{aligned}\langle\hat{O}_m\hat{P}_n\hat{Q}_k\rangle &= \langle\Delta\hat{O}_m\Delta\hat{P}_n\Delta\hat{Q}_k\rangle \\ &+ \langle\hat{O}_m\rangle\langle\Delta\hat{P}_n\Delta\hat{Q}_k\rangle + \langle\hat{P}_n\rangle\langle\Delta\hat{O}_m\Delta\hat{Q}_k\rangle \\ &+ \langle\Delta\hat{O}_m\Delta\hat{P}_n\rangle\langle\hat{Q}_k\rangle + \langle\hat{O}_m\rangle\langle\hat{P}_n\rangle\langle\hat{Q}_k\rangle. \end{aligned} \tag{36}$$

It separates into the three-site correlation of quantum fluctuations $\langle\Delta\hat{O}_m\Delta\hat{P}_n\Delta\hat{Q}_k\rangle$ and into lower correlation functions. Now, the suggested approximation and just the truncation of the hierarchy of kinetic equations is based on the neglect of this three-site correlation of quantum fluctuations. We will apply this approximation to all three-site functions which appear in the equations of motion of the two-site functions. The factorization into products of lower order functions also
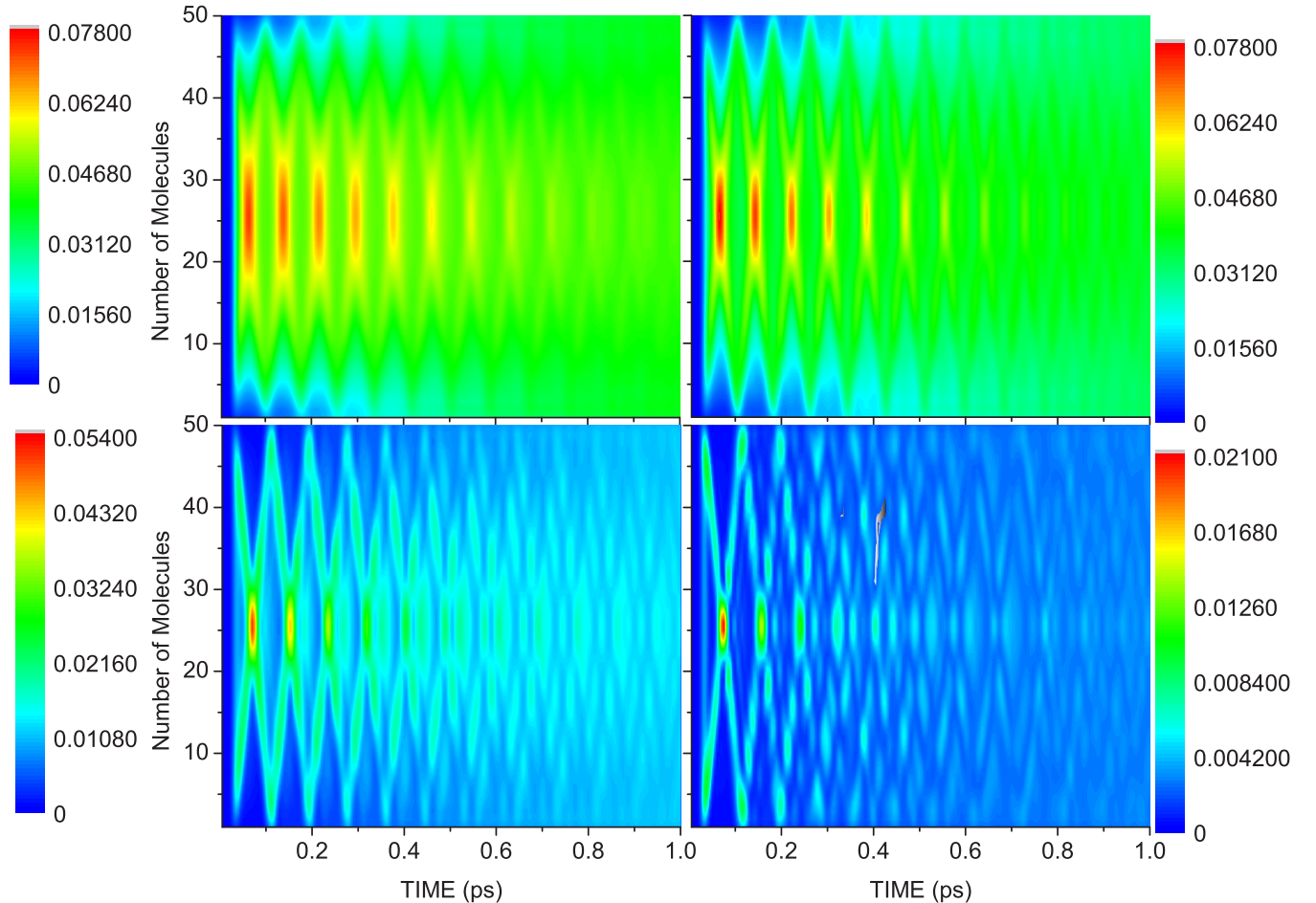

FIG. 5. Molecular excited-state populations P_m versus time for a chain of 50 6P molecules and a laser pulse excitation with $E_0 = 2.5 \times 10^7$ V/m and $\tau_p = 20$ fs ($t_p = 30$ fs, $k = 2 \times 10^{11}$/s). Variation of photon energy $\hbar\omega_0$; upper left panel: $\hbar\omega_0 = 4.318$ eV; upper right panel: $\hbar\omega_0 = 4.275$ eV; lower left panel: $\hbar\omega_0 = 4.22$ eV; lower right panel: $\hbar\omega_0 = 4.17$ eV.
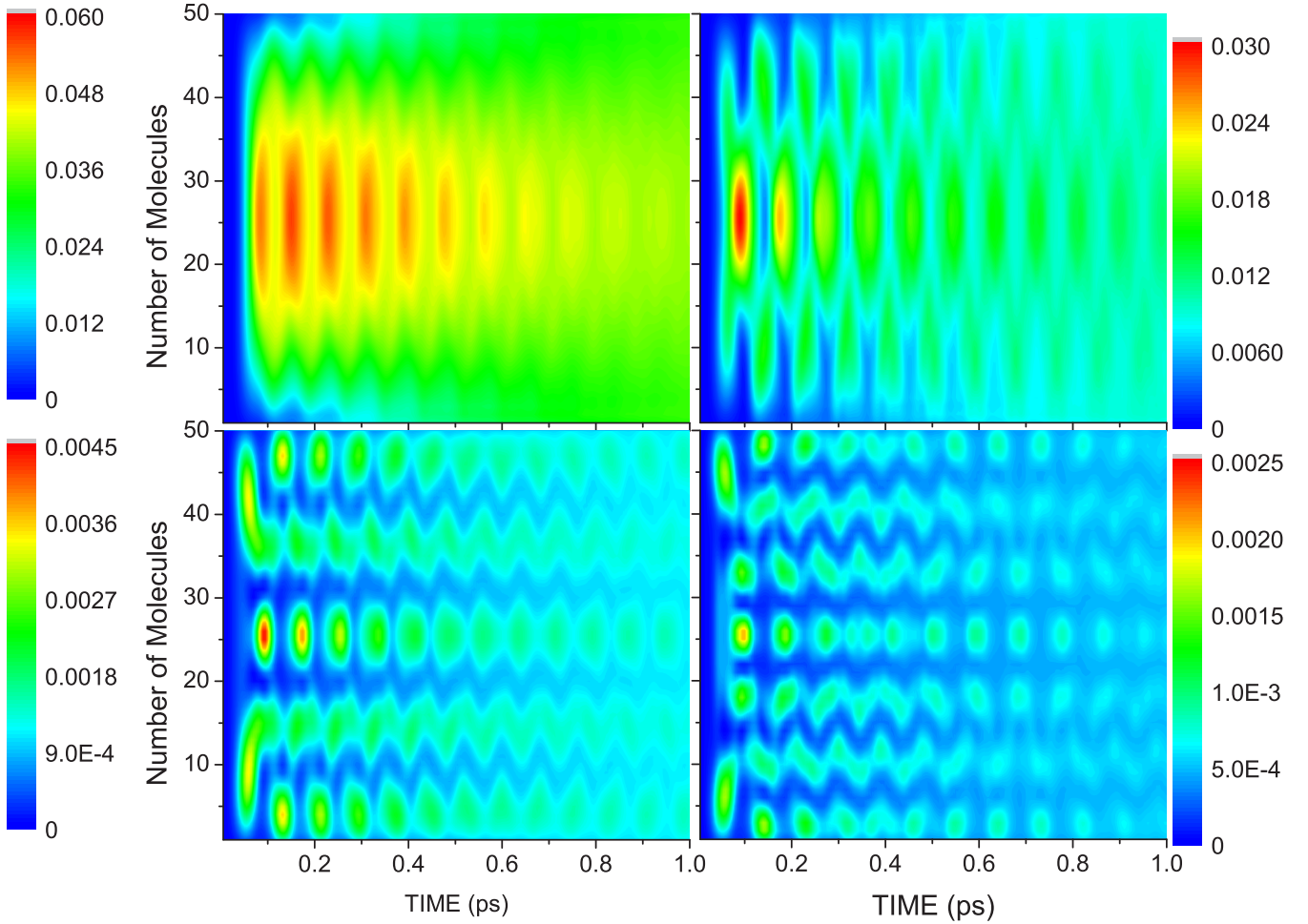
FIG. 6. Molecular excited-state populations P_m versus time for a chain of 50 6P molecules and a laser pulse excitation with $E_0 = 10^7$ V/m and $\tau_p = 50$ fs ($t_p = 70$ fs, $k = 2 \times 10^{11}$/s). Variation of photon energy as in Fig. 5.

indicates that in the general case the approximation scheme corresponds to an expansion with respect to the excitation density.

We notice Eq. (35) and define the correlated part of the two-site functions according to

$$K_{km}(t) = \langle B_k^+ B_m^+ B_m \rangle - A_k(t) P_m(t), \tag{37}$$

$$W_{mn}(t) = \langle B_m^+ B_n \rangle - A_m(t) A_n^*(t), \tag{38}$$

$$B_{mn}(t) = \langle B_m^+ B_n^+ \rangle - A_m(t) A_n(t), \tag{39}$$

and

$$R_{km}(t) = \langle B_k^+ B_k B_m^+ B_m \rangle - P_k(t) P_m(t). \tag{40}$$

Utilizing all these relations, the three-site correlation functions can be expressed by the single-site functions A_m, P_m and the correlated parts of the two-site functions K_{km}, W_{mn}, B_{mn}, and R_{km}. Related kinetic equations are discussed next.

D. Set of kinetic equations—coherent part

As already indicated, equations of motion for single-site functions are given in Ref. [37]. To get equations of motion

for the correlated parts of the two-site functions, we notice

$$\frac{\partial}{\partial t} \langle \Delta \hat{O}_m \Delta \hat{P}_n \rangle = \frac{\partial}{\partial t} \langle \hat{O}_m \hat{P}_n \rangle$$
$$- \left(\frac{\partial}{\partial t} \langle \hat{O}_m \rangle \right) \langle \hat{P}_n \rangle - \langle \hat{O}_m \rangle \left(\frac{\partial}{\partial t} \langle \hat{P}_n \rangle \right). \tag{41}$$

Hence, the equations of motion for the two-site functions $\langle \hat{O}_m \hat{P}_n \rangle$ listed in Ref. [37] have to be rearranged according to the above given scheme. Moreover, the relation Eq. (41) can be specified for the coherent and dissipative parts of the equation of motion.

To quote the results of the respective computations, we introduce $\omega_m = E_m/\hbar$, $v_{mn} = V_{mn}/\hbar$, $j_{mn} = J_{mn}/\hbar$, and $r_m = R_m/\hbar$. Note that we offer here only the equations for the two single-site functions but include the separations Eqs. (37)–(40) of the two-site functions. All relations for the two-site functions are found in Ref. [37]. And, equations of motion for the approximate set of single-site and two-site functions used for the study of the 6P molecular systems are quoted in the next section.
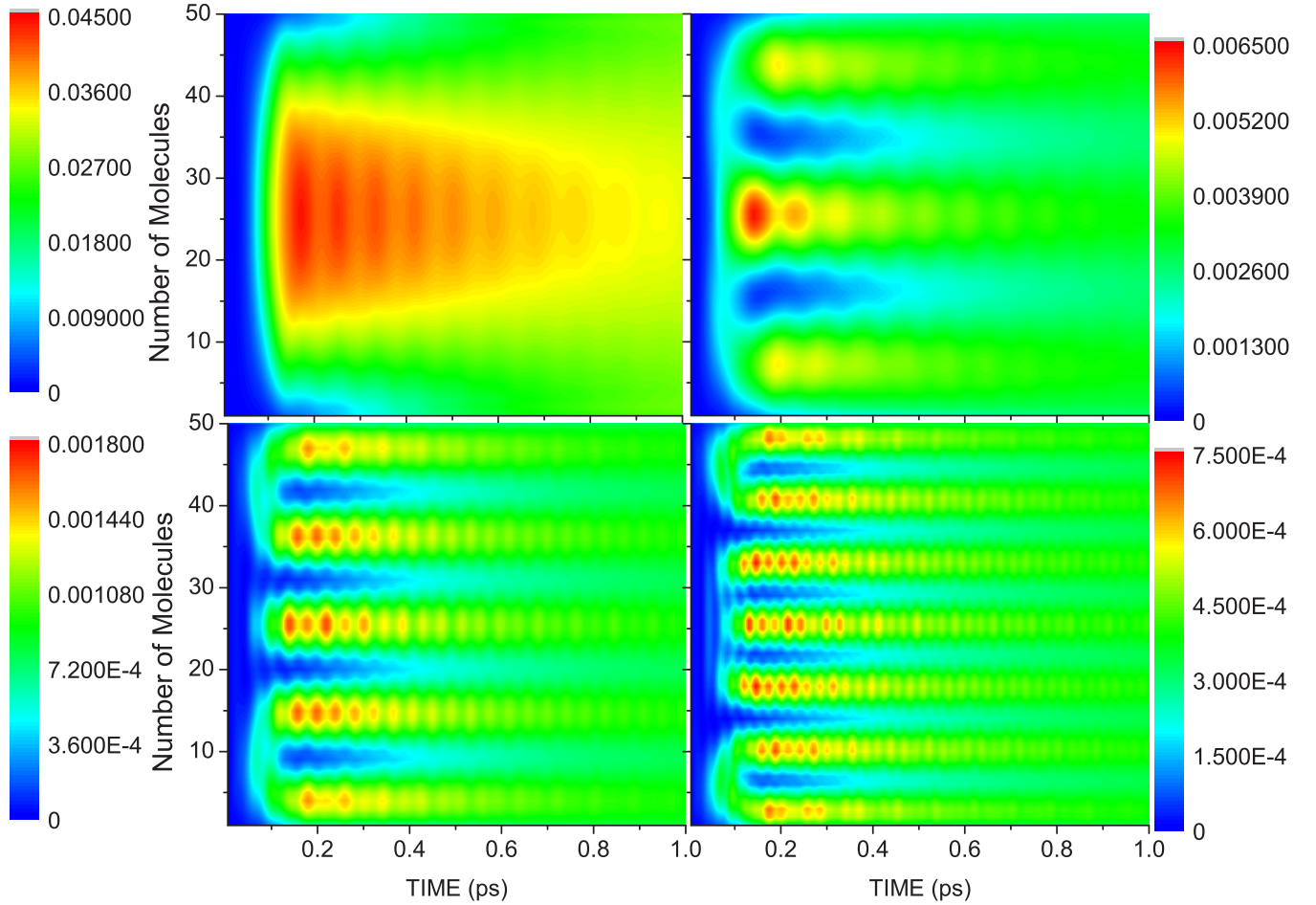
FIG. 7. Molecular excited-state populations P_m versus time for a chain of 50 6P molecules and a laser-pulse excitation with $E_0 = 5 \times 10^6$ V/m and $\tau_p = 100$ fs ($t_p = 80$ fs, $k = 2 \times 10^{11}$/s). Variation of photon energy as in Fig. 5.

We get for the transition amplitude

$$\left(\frac{\partial A_m}{\partial t}\right)_{\text{coh}} = i\omega_m A_m + 2i\sum_k v_{km}(K_{mk} + A_m P_k) + ir_m^*[1 - 2P_m]$$

$$+ i\sum_k j_{km}(A_k[1 - 2P_m] - 2K_{km}). \quad (42)$$

As in the subsequent equations, the term proportional to v_{mn} describes the Coulomb shift of molecular energies due to the actual degree of excitation. This shift is also originated by the function K_{mk}, which correlates excitation of molecule m and excited-state population of molecule k. The coupling to the radiation field as well as the last term in Eq. (42) is affected by $1 - 2P_m$, which is identical to the population inversion $P_{mg} - P_{me}$. If in the final state of an EET process $P_{mg} = P_{me}$, excitation and de-exciton are equally probable and a net transfer does not take place.

To get an equation for P_m, we arrive at

$$\left(\frac{\partial P_m}{\partial t}\right)_{\text{coh}} = -i\sum_q j_{mq}[W_{mq} + A_m A_q^*] - ir_m A_m + \text{c.c.}$$

$$(43)$$

The function W_{mq} is the only two-site function which enters the equation. This indicates that the consideration of W_{mq} is

essential for EET which is not directly connected with optical induced formation of the transition amplitudes A_m. Such a direct optical excitation of the molecules is achieved by the terms $\sim r_m$. We also note that the different nonlinear terms indicate the deviation from simple single-exciton kinetics.

E. Set of kinetic equations—dissipative part

It follows for the transition amplitudes:

$$\left(\frac{\partial A_m}{\partial t}\right)_{\text{diss}}$$

$$= -\left(\frac{\kappa_m}{2} + \gamma_m^{(\text{pd})} + \frac{1}{2}\sum_q k_{m \to q}(1 - P_q) + \frac{1}{2}\sum_q k_{q \to m}P_q\right)A_m$$

$$+ \frac{1}{2}\sum_q (k_{m \to q} - k_{q \to m})K_{mq}. \quad (44)$$

Excited state decay, pure dephasing, and vibrational-assisted EET constitute the complete dephasing rate. In the case of EET, transitions from the considered molecule m to other ones are distinguished from the reverse process (factor $1 - P_q$ and P_q, respectively). A separate term is formed by the two-site function K_{mq}.
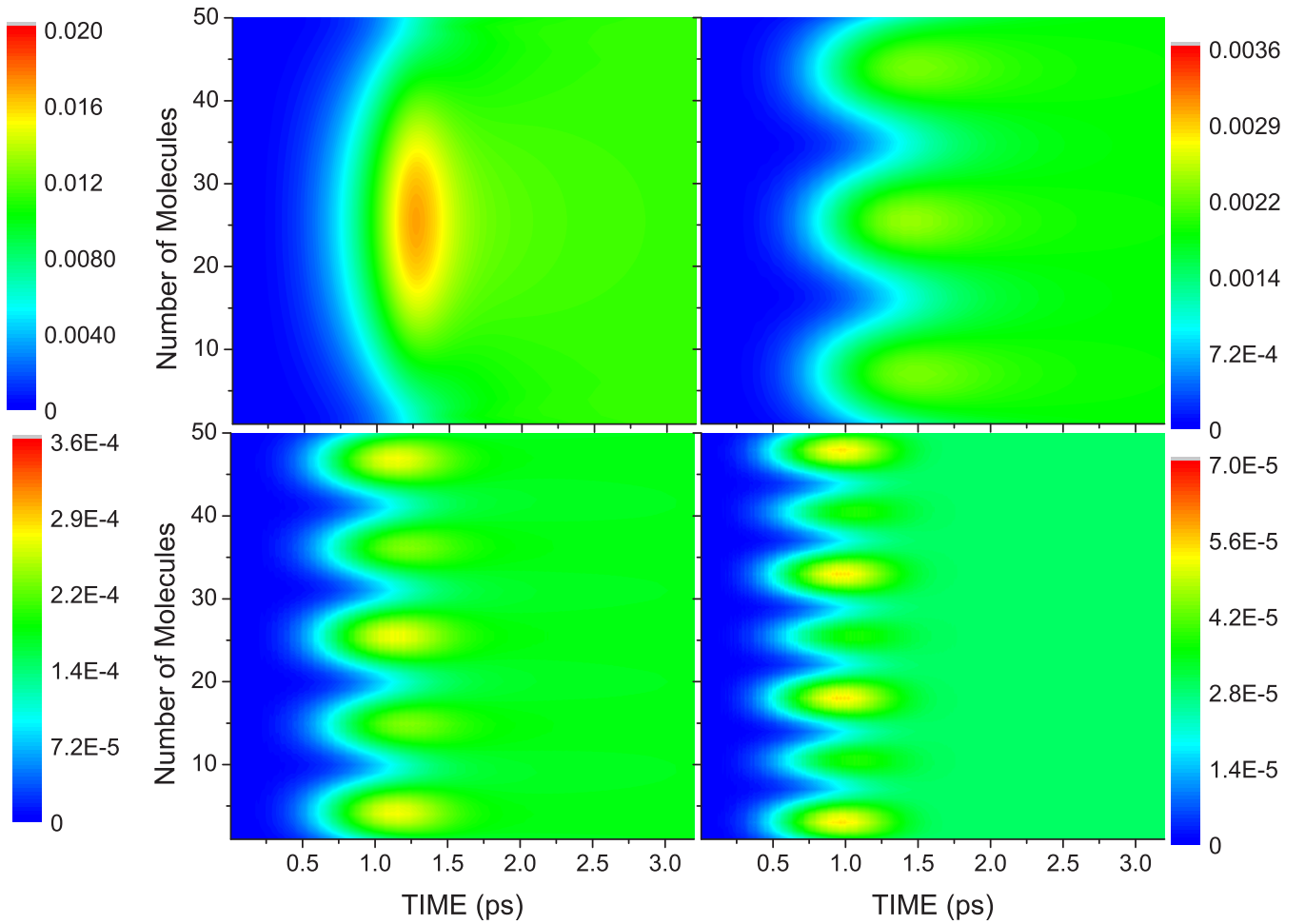
FIG. 8. Molecular excited-state populations P_m versus time for a chain of 50 6P molecules and a laser-pulse excitation with $E_0 = 5 \times 10^5$ V/m and $\tau_p = 1$ ps ($t_p = 0.8$ ps, $k = 2 \times 10^{11}$/s). Variation of photon energy as in Fig. 5.

Vibrational-assisted EET also dominates the equation of motion for the excited-state population:

$$\left(\frac{\partial P_m}{\partial t}\right)_{\text{diss}} = -\kappa_m P_m - \sum_q k_{m \to q} P_m (1 - P_q)$$
$$+ \sum_q k_{q \to m} P_q (1 - P_m) - \sum_q (k_{m \to q} - k_{q \to m}) R_{mq}. \tag{45}$$

The P_m are arranged according to a standard rate equation. Concerning equations for the two-site functions, we again refer to Ref. [37].

IV. MULTIEXCITON DYNAMICS IN *PARA*-SEXIPHENYL CLUSTERS

Para-sexiphenyl (6P) clusters of different shapes have been discussed by us recently in Refs. [31–33]. It could be demonstrated that charge-transfer contributions to the excited state description of 6P clusters are of less importance. Accordingly the EET model introduced here would be very appropriate. We will consider optical excitation and subsequent EET in 1D and 2D structures of about 50 6P molecules. The different types of spatial arrangements and EET coupling results in distinct Coulomb shifts and exciton spectra. Figure 2 displays

50 π-stacked 6P molecules which form a H-aggregate (cf. Refs. [31–33]). A possible 2D structure is shown in Fig. 3. The typical herringbone structure is formed if the 6P molecules are arranged, for example, at a wurtzite (0001) ZnO surface [34–36]. Figure 4 displays the electrostatic shift of 59 molecular disks.

A particular aim will be the consideration of Coulomb-shift effects and of excitation energy relaxation processes due to the involved vibrational-assisted EET. Because of these specific tasks, we do not work with the complete system of two-site functions. As demonstrated in Ref. [25], the consideration of W_{mn} alone offers a nearly correct description of the system.

The rates of vibrational-assisted EET are taken as constants which only connect closely positioned 6P molecules. We set $k_{m \to n} = k_{n \to m} \equiv k = 10^{11}...10^{12}$/s. A more involved description is a work in progress (see also Table I).

We quote respective kinetic equations. Since the rates of excited decay are much smaller than the $k_{m \to n}$, we ignore the κ_m. For the same reason, we also neglect the pure dephasing rates. It follows for the transition amplitude:

$$\frac{\partial}{\partial t} A_m = i\tilde{\Omega}_m A_m + i \sum_k (1 - 2P_m) j_{mk} A_k + i r_m^* (1 - 2P_m). \tag{46}$$
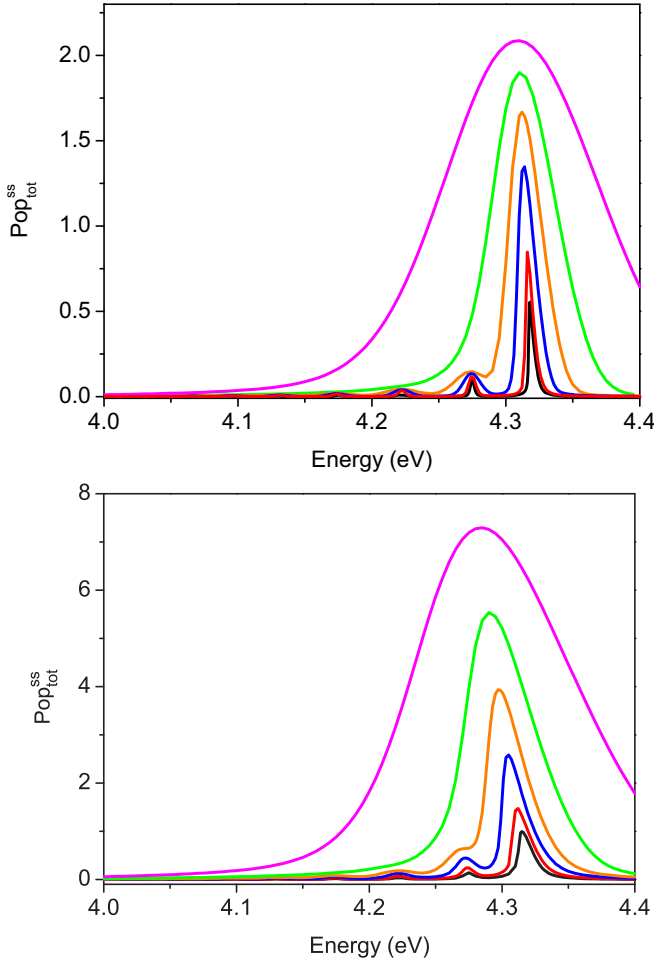
FIG. 9. Steady-state value $P_{\mathrm{tot}}^{(\mathrm{ss})}$ of the total excitation of a chain of 50 6P molecules drawn versus the photon energy $\hbar\omega_0$ of the exciting laser pulse. Variation of the pulse duration τ_p. Upper panel: $a_p = 5 \times 10^5$ ps V/m, $k = 2 \times 10^{11}$/s; lower panel: $a_p = 10^6$ ps V/m and $k = 10^{12}$/s. Black line: $\tau_p = 1$ ps, red line: $\tau_p = 500$ fs, blue line: $\tau_p = 200$ fs, orange line: $\tau_p = 100$ fs, green line: $\tau_p = 50$ fs, purple line: $\tau_p = 20$ fs.

Note the introduction of the complex frequency:

$$\tilde{\Omega}_m = \omega_m + 2 \sum_n v_{mn} P_n$$
$$+ \frac{i}{2} \sum_n \left(k_{m \to n}(1 - P_n) + k_{n \to m} P_n \right). \quad (47)$$

It covers the excitation energy of molecule m,

$$E_m + 2 \sum_n V_{mn} P_n$$
$$= E_{me} + \sum_n \left(J_{mn}(ee, gg) P_{ng} + J_{mn}(ee, ee) P_{ne} \right)$$
$$- E_{mg} - \sum_n \left(J_{mn}(gg, gg) P_{ng} + J_{mn}(gg, ee) P_{ne} \right), \quad (48)$$

which is Coulomb shifted due to the actual degree of excitation (note the use of $P_n = P_{ne}$ and $1 - P_n = P_{ng}$).

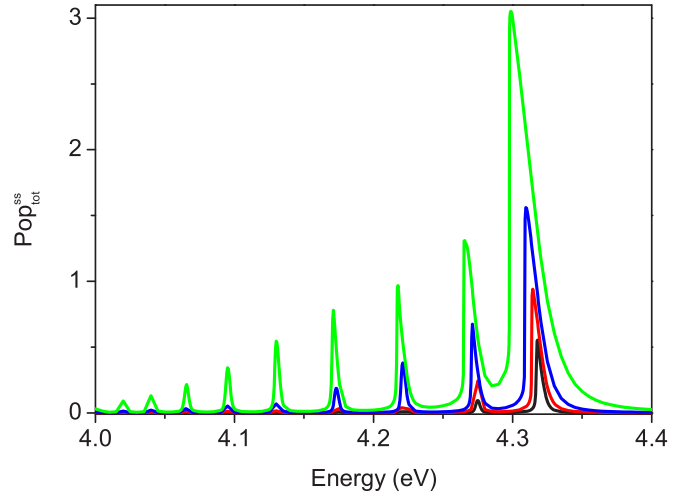FIG. 10. Steady-state value $P_{\mathrm{tot}}^{(\mathrm{ss})}$ of the total excitation of a chain of 50 6P molecules drawn versus the photon energy $\hbar\omega_0$ of the exciting laser pulse. Variation of the pulse amplitude E_0 ($\tau_p = 1$ ps, $k = 2 \times 10^{11}$/s). Black line: $E_0 = 5 \times 10^5$ V/m; red line: $E_0 = 10^6$ V/m; blue line: $E_0 = 2 \times 10^6$ V/m; green line: $E_0 = 5 \times 10^6$ V/m.

For the excited-state populations, we obtain

$$\frac{\partial}{\partial t} P_m = 2\mathrm{Im} \sum_q j_{mq}(W_{mq} + A_m A_q^*) + 2\mathrm{Im} r_m A_m$$
$$- \sum_q (k_{m \to q} P_m (1 - P_q) - k_{q \to m} P_q (1 - P_m)),$$

$$(49)$$

and, finally, we have for W_{mn}:

$$\frac{\partial}{\partial t} W_{mn} = \left(i(\tilde{\Omega}_m - \tilde{\Omega}_n^*) - \frac{1}{2} k_{m \to n}(1 - P_m) \right.$$
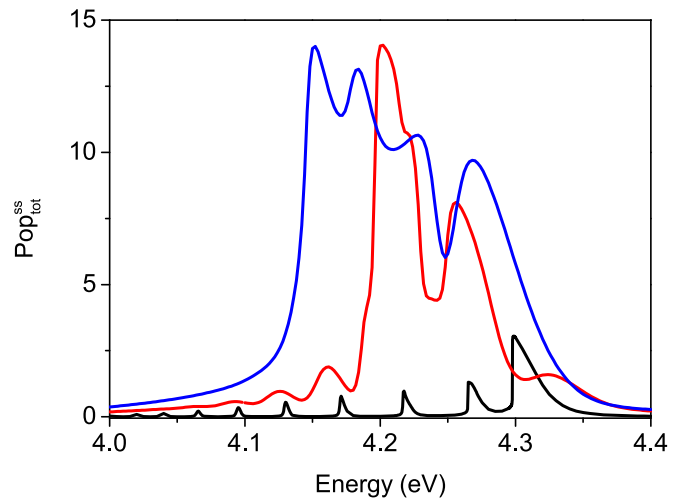$$\left. - \frac{1}{2} k_{n \to m}(1 - P_n) \right) W_{mn} - i j_{nm}(P_m - P_n)$$

FIG. 11. Steady-state value $P_{\mathrm{tot}}^{(\mathrm{ss})}$ of the total excitation of a chain of 50 6P molecules drawn versus the photon energy $\hbar\omega_0$ of the exciting laser pulse at $a_p = 5 \times 10^6$ ps V/m and $k = 2 \times 10^{11}$/s. Variation of the pulse duration τ_p. Black line: $\tau_p = 1$ ps; red line: $\tau_p = 100$ fs; blue line: $\tau_p = 50$ fs.
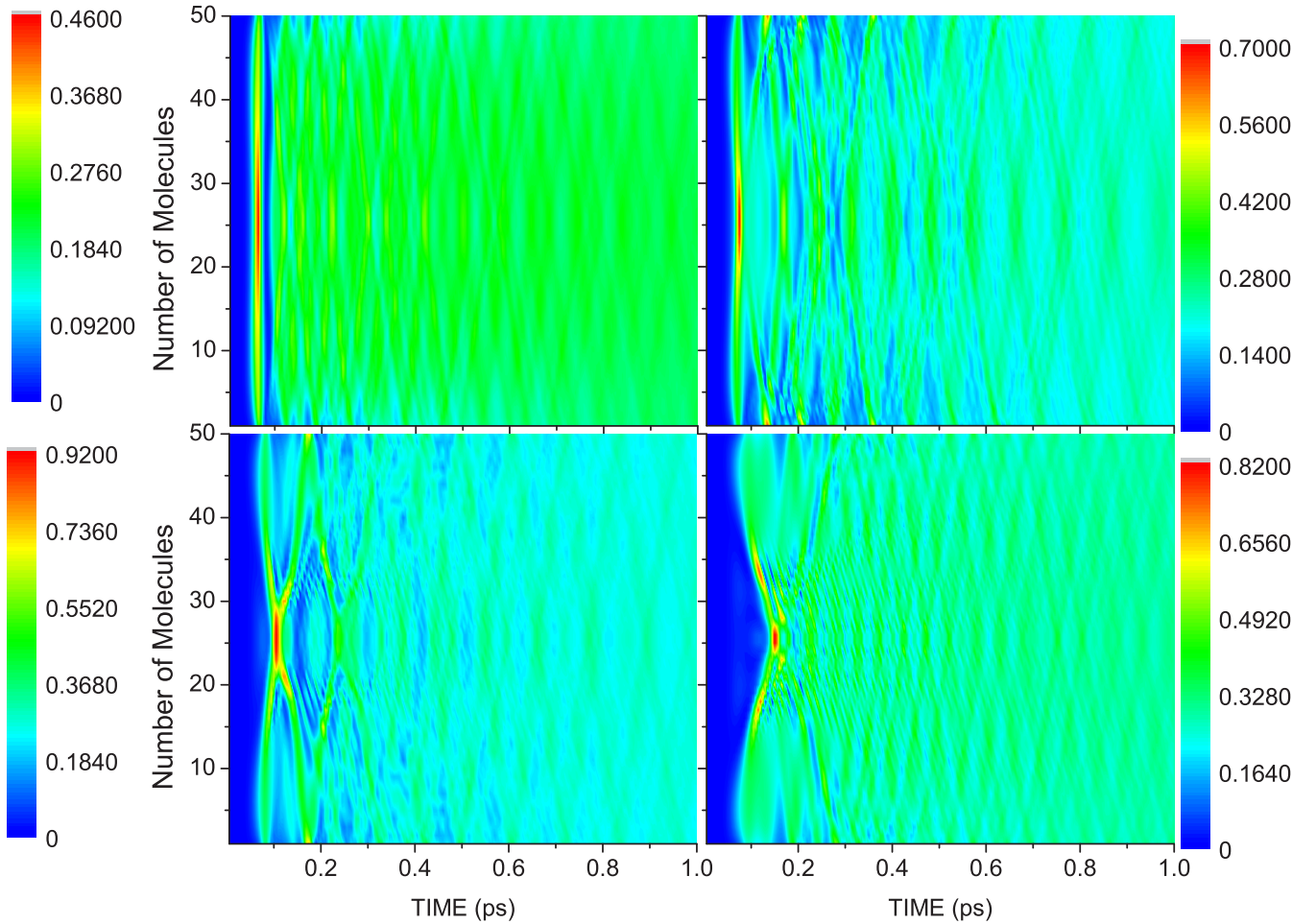
FIG. 12. Molecular excited-state populations P_m versus time for a chain of 50 6P molecules and a laser-pulse excitation with $E_0 = 10^8$ V/m and $\tau_p = 50$ fs ($t_p = 70$ fs, $k = 2 \times 10^{11}/$s). Variation of photon energy. $\hbar\omega_0 = 4.268$ eV (upper left), 4.23 eV (upper right), 4.184 eV (lower left), 4.152 eV (lower right).

$$+i\sum_{k\neq m,n}(j_{km}W_{kn}(1-2P_m) - j_{nk}W_{mk}(1-2P_n))$$

$$+ij_{nm}A_mA_m^*(1-2P_n) - ij_{nm}(1-2P_m)A_nA_n^*$$

$$-\frac{1}{2}\{k_{m\to n} + k_{n\to m}$$

$$-(k_{m\to n} - k_{n\to m})(P_m - P_n)\}A_mA_n^*. \tag{50}$$

Appropriate quantities for an analysis of the photoinduced kinetics are the excited-state populations P_m and also the transition amplitudes A_m. Remember also that the single appearance of W_{mq} in the equation for P_m is important for a correct description of EET.

In line with Ref. [24], we also compute the steady-state value of the total excitation:

$$P_{\text{tot}}^{(ss)} = \sum_m P_m^{(ss)}. \tag{51}$$

Since the excited state lifetime of 6P molecules is in the nanosecond range, the steady-state values $P_m^{(ss)}$ of the excited state populations formed after femtosecond optical excitations are well-defined quantities on the picosecond timescale. As described in Ref. [24], these quantities can be measured in a sequential pump-probe experiment. If $P_{\text{tot}}^{(ss)}$ is drawn versus

photon energy $\hbar\omega_0$ of laser pulse excitation, particular insight related to the multi-exciton states can be obtained (cf. also Ref. [24]).

A. 1D 6P clusters

We already introduced the 6P 1D cluster of interest. Besides the molecular structure, Fig. 2 displays the electrostatic shift of the individual molecular excitation energies $E_{me} - E_{mg}$ [cf. Eq. (10)]. The single exciton energies are also drawn. The electrostatic shift is somewhat below 10 meV while the exciton band covers a range of about 0.4 eV. The negative values of the electrostatic shift of the individual 6P energies reveal the attractive character of the related force. It is of less importance if the Frenkel-exciton spectrum is considered. Nevertheless, all computations have been carried out using the energies, Eq. (10), and the excitation dependent corrections, Eq. (11). According to the H-aggregate character of the 6P chain, the upper exciton level has the largest oscillator strength. It is followed by the third level, the fifth level, and so on.

We start our analysis with a set of figures which display the excited-state formation due to laser-pulse excitation of different durations. Therefore, all P_m are drawn versus time.
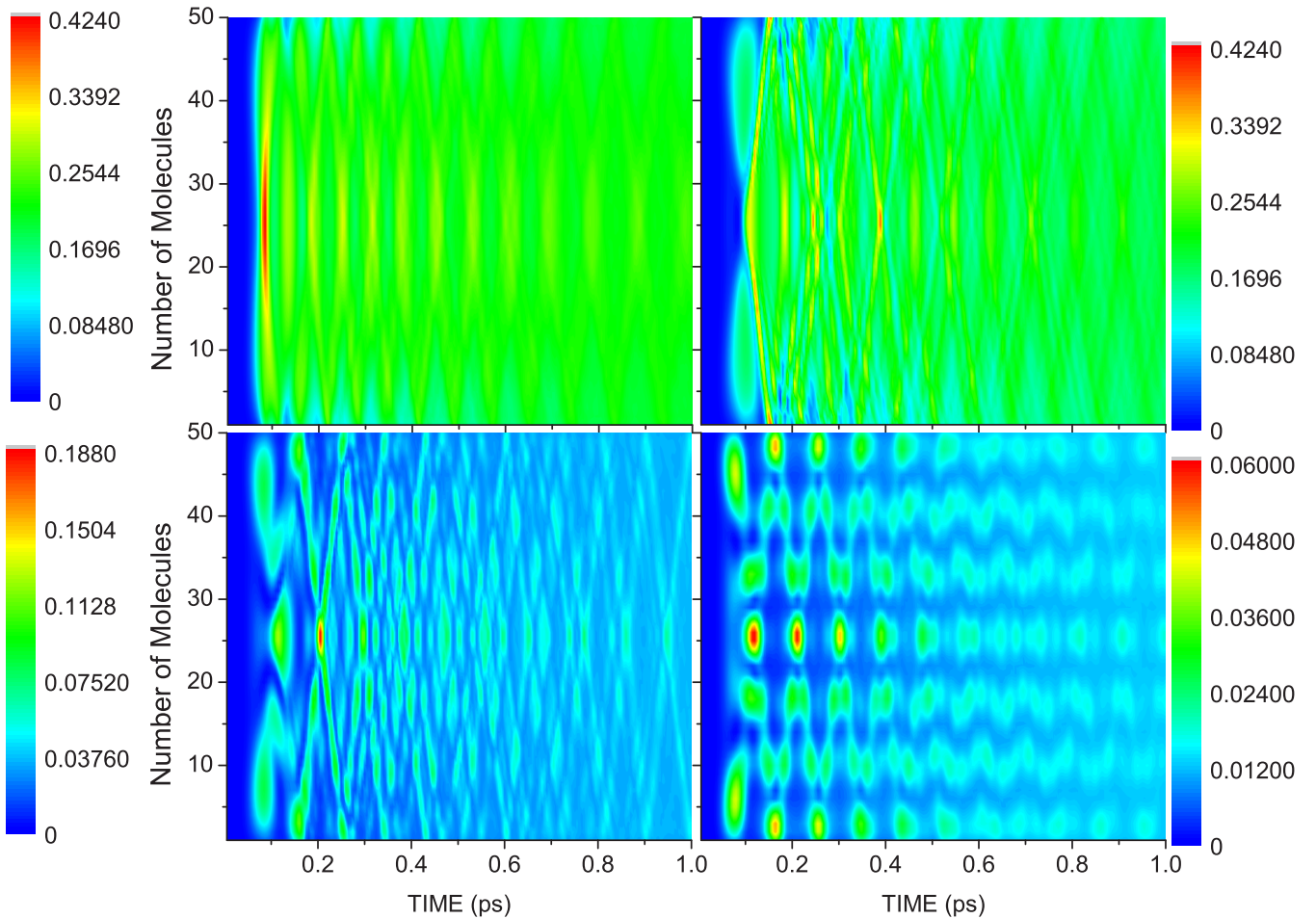
FIG. 13. Molecular excited-state populations P_m versus time for a chain of 50 6P molecules and a laser pulse excitation with $E_0 = 5 \times 10^7$ V/m and $\tau_p = 100$ fs ($t_p = 80$ fs, $k = 2 \times 10^{11}$/s). Variation of photon energy. $\hbar\omega_0 = 4.256$ eV (upper left), 4.222 eV (upper right), 4.2 eV (lower left), 4.162 eV (lower right).

For an efficient presentation, we chose here and in all subsequent figures a contour plot. To do this, we interpolated the discrete values which belong to the different molecules and obtain a continuous presentation. Figure 5 corresponds to the consideration of a 20-fs-long laser pulse, Fig. 6 to a 50-fs-long pulse, Fig. 7 to 100-fs-long pulse, and Fig. 8 to a 1-ps-long pulse. The related spectral broadening of the pulse can be estimated as $\hbar/\tau_p$ and takes the values of about 33 meV, 13 meV, 6 meV, and 0.6 meV, respectively. To make the different examples comparable to each other, the field-amplitude E_0, Eq. (18), is chosen to obtain a single value of $a_p = \tau_p E_0$. This quantity represents a measure for the so-called pulse area and amounts to 5×10^5 ps V/m here. As becomes obvious from the absolute values of the P_m in Figs. 5 to 8, all examples correspond to the case of weak excitation.

In every figure, the used photon energies equal the first exciton level, the third level (from above), the fifth, and the seventh level (cf. Fig. 2). Those are the first four bright levels (see below). Their energetic distance overcomes even the spectral broadening of the shortest pulse. We cannot expect a pronounced wave-packet formation for the longer pulses but the population of mainly a single exciton level.

This is best seen at the sequence of four pictures corresponding to the 1-ps-long excitation (cf. Fig. 8). According to the number of nodes of the exciton wave function (zero, two, four, and six), the long but spectral sharp excitation originates a single population structure, as well as three, five, and seven structures, respectively. They are stable along laser-pulse excitation (and somewhat longer) and decay to form a rather homogeneous excitation distribution in the chain. EET only appears in the step of the formation of this final homogeneous excitation and is mainly originated by the chosen type of dissipation.

Turning to the case of a 100-fs-long excitation (cf. Fig. 7), oscillations of the P_m are visible in the part where the populations are maximal. The larger spectral broadening of the pulse compared to the forging one let neighboring exciton levels interfere a little bit and form a wave packet. This effect is more pronounced for the 50- and 20-fs pulses. In particular, for the shortest pulse, the central part of the chain gets excited and then the excitation moves to the two ends of the chain to be reflected and to move back. This process extends over several hundreds of fs. It indicates noticeable wave-packet formation, but in a linear regime of excitation.

To improve the understanding of the foregoing figures, we discuss the related steady-state value $P_{\text{tot}}^{(ss)}$ of the total chain
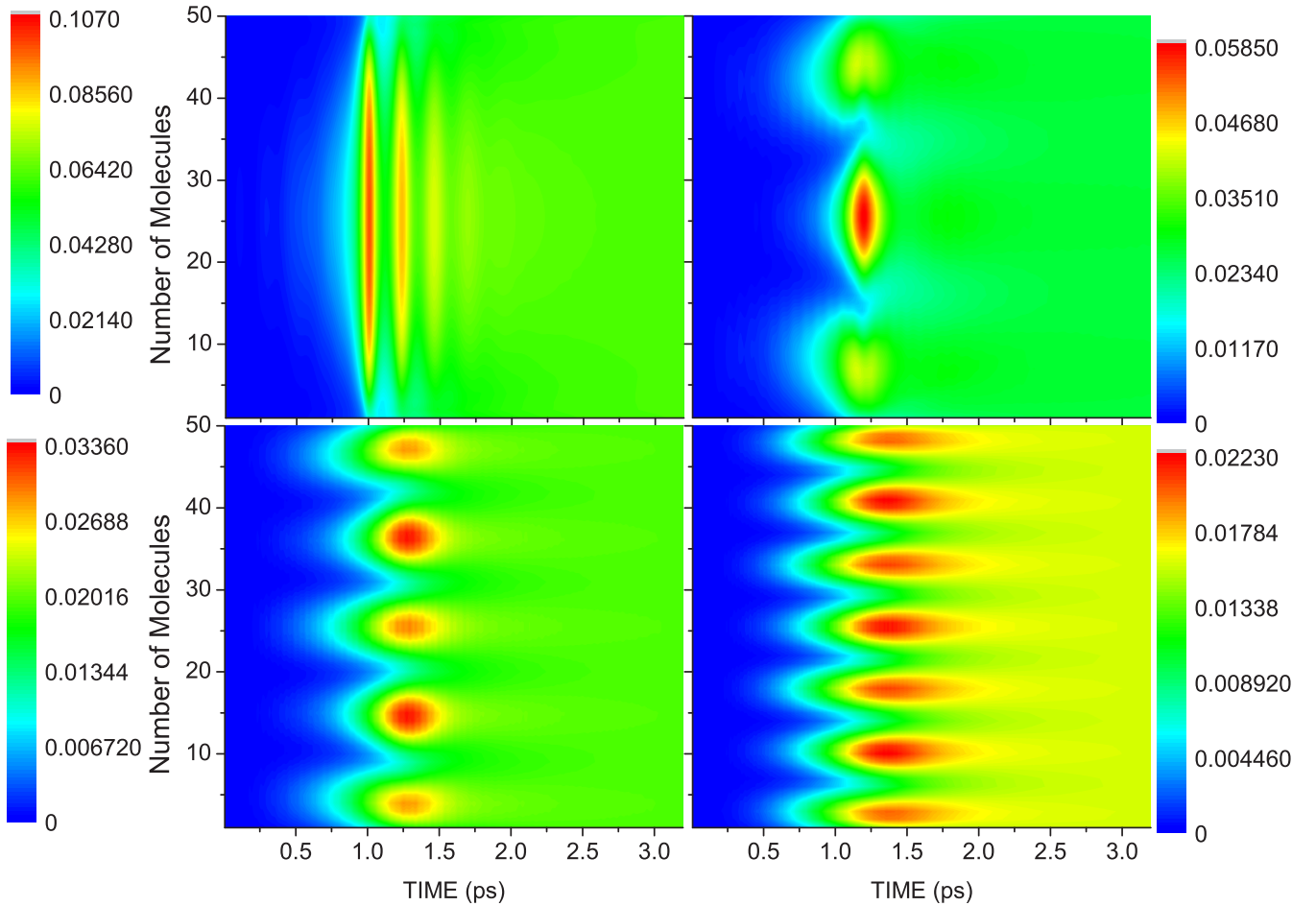
FIG. 14. Molecular excited-state populations P_m versus time for a chain of 50 6P molecules and a laser pulse excitation with $E_0 = 5 \times 10^6$ V/m and $\tau_p = 1$ ps ($t_p = 0.8$ ps, $k = 2 \times 10^{11}$/s). Variation of photon energy. $\hbar\omega_0 = 4.2987$ eV (upper left), 4.2655 eV (upper right), 4.2175 eV (lower left), 4.171 eV (lower right).

excitation Eq. (51). The upper part of Fig. 9 corresponds to the a_p value used beforehand (to have some broader structures, we increased the rate k somewhat). Again we indicate that we work in the regime of linear excitation since $P_{tot}^{(ss)}$ (corresponding to 50 molecules) stays around the value 1.

The curves corresponding to the three longest pulses reproduce the linear absorption spectrum with peaks at the energetic position of the odd exciton levels (counted from above). The increasing spectral broadening going along with a decreasing pulse duration results in a broadening of the peak structures related to $P_{tot}^{(ss)}$ (complete resonance with the odd exciton levels is not necessary for excitation). Changing to pulses of 100-fs duration and less, the peak structure of $P_{tot}^{(ss)}$ is lost. This observation goes along with the temporal behavior of the P_m for the case of a 20-fs excitation (cf. Fig. 5). The spectral broad character of the excitation forms a wave packet which results in a main population of the central part of the chain.

While the peak positions of $P_{tot}^{(ss)}$ versus $\hbar\omega_0$ stay constant for the case of $a_p = 5 \times 10^5$ ps V/m, they do not for the used higher a_p value (lower panel of Fig. 9). Decreasing the pulse duration, and by that, increasing the field-amplitude E_0 and the total value of $P_{tot}^{(ss)}$, the peak positions move to lower energies. This can be interpreted as a multiexciton effect [24].

Increasing the degree of excitation, the population inversion $1 - 2P_m$ starts to noticeable deviate from 1. Accordingly, the resulting effective EET coupling $(1 - 2P_m)j_{mk}$ appearing in Eq. (46) for A_m and Eq. (50) for W_{mn} is reduced. A shrinkage of the exciton spectrum results and, in the case of a H-aggregate configuration, the visible upper exciton levels move to lower energies (red shift).

A similar explanation is possible when using the right scheme of Fig. 1, showing multiexciton bands. When climbing the ladder of multiexciton bands upward, the bandwidth gets larger. Consequently, if nonlinear absorption becomes possible, single photon transitions between higher lying multiexciton bands appear. According to the band broadening, the necessary photon energies get smaller and the overall absorption peak may move to lower energies.

The same low-energy shifts of the $P_{tot}^{(ss)}$ curves are shown in Fig. 10 for 1-ps-long pulses but different field amplitudes E_0. Since the pulses are spectrally sharp compared to the shorter ones used in the foregoing figure, there is no considerable broadening with increasing E_0. However, the redshift of the highest peaks and the following peaks are obvious. But the decreasing excited state population with decreasing photon energy suppresses the multiexciton effect for lower lying peaks (the related $P_{tot}^{(ss)}$ values are too small).
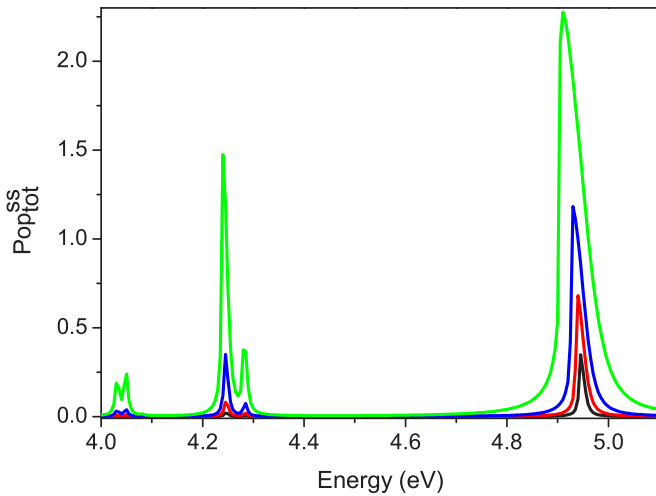
FIG. 15. Steady-state value $P_{\text{tot}}^{(\text{ss})}$ of the total excitation of a disk of 59 6P molecules drawn versus the photon energy $\hbar\omega_0$ of the exciting laser pulse. Variation of the field strength E_0, $\tau_p = 1$ ps, $k = 10^{12}$/s. Black line: $E_0 = 5 \times 10^5$ V/m; red line: $E_0 = 10^6$ V/m; blue line: $E_0 = 2 \times 10^6$ V/m; green line: $E_0 = 5 \times 10^6$ V/m.

B. Regime of nonlinear transport

By analyzing the steady-state values $P_{\text{tot}}^{(\text{ss})}$ of the total excitation in the foregoing section, we already met multiexciton effects, i.e., effects of nonlinear EET. Here, we continue this analysis. Figure 11 displays $P_{\text{tot}}^{(\text{ss})}$ versus photon energy for $a_p = 5 \times 10^6$ ps V/m, a value larger than those used for Fig. 9. According to the increased a_p value, total excitations of the chain larger than ten are obtained and the peak structure of $P_{\text{tot}}^{(\text{ss})}$ is strongly deformed compared with the low-excitation one. Here, it remains an open question if the used degree of excitation corresponds to the described truncation of the hierarchy of kinetic equations. Respective studies are work in progress.

Figures 12–14 show the temporal behavior of the respective excited-state populations P_m. Note that the actual photon energies $\hbar\omega_0$ are chosen according to the actual peak position of $P_{\text{tot}}^{(\text{ss})}$ in Fig. 11. These P_m need to be compared with those of the weak excitation case represented by Figs. 6, 7, and 8.

Starting with the case of $\tau_p = 1$ ps, the P_m plots in Figs. 14 and 8 belonging to the lower photon energies looks similar. However, the case of the highest photon energy at 4.2987 eV looks different. Distinct Rabi-like oscillations of the P_m in the central part of the chain are visible before EET results in an uniform excitation of the whole chain. Rabi-like oscillations of the P_m are also visible for 50-fs and 100-fs pulse duration (Figs. 12, 13, respectively). An excitation distribution as in the case of low excitation reflecting the node structure of the underlying exciton wave function is not visible.

C. 2D 6P clusters

The 2D structure of the 6P molecules being of interest for the following has been already introduced in Fig. 3. The shift of the excitation energies due to intermolecular electrostatic interactions are shown in Fig. 4. The shift covers values up to 15 meV. Due to the herringbone structure of the molecular
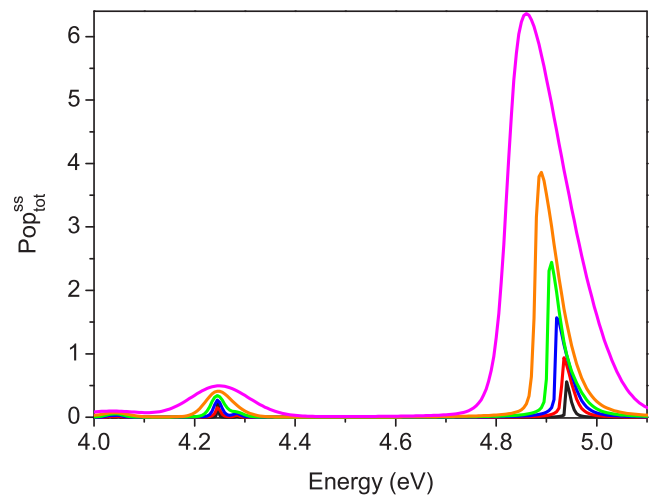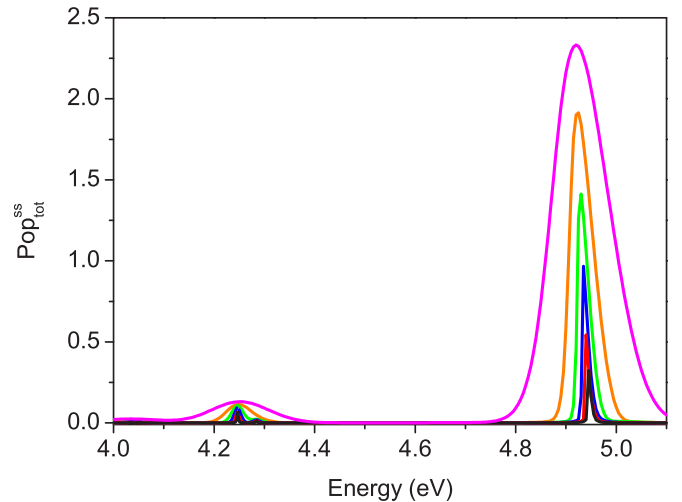

FIG. 16. Steady-state value $P_{\text{tot}}^{(\text{ss})}$ of the total excitation of a disk of 59 6P molecules drawn versus the photon energy $\hbar\omega_0$ of the exciting laser pulse. Variation of the pulse duration τ_p. Upper panel: $a_p = 5 \times 10^5$ ps V/m, $k = 2 \times 10^{11}$/s; lower panel: $a_p = 10^6$ ps V/m, $k = 2 \times 10^{11}$/s. Black line: $\tau_p = 1$ ps; red line: $\tau_p = 500$ fs; blue line: $\tau_p = 200$ fs; green line: $\tau_p = 100$ fs; orange line: $\tau_p = 50$ fs; purple line: $\tau_p = 20$ fs.

arrangement in the disk, the electrostatic shift decreases from the central part to the edge. Again, the influence on the exciton spectrum (right panel of Fig. 4) is less pronounced. As expected, the Frenkel exciton-level structure is different from the 1D case, Fig. 2, and its bandwidth amounts to more than 1 eV. Due to closer packing and 2D EET coupling among the 6P molecules in the disk, the bandwidth strongly overcomes the one formed by the regular 1D chain structure.

To characterize linear and nonlinear absorption and, thus, multiexciton effects, we again calculate the steady-state value $P_{\text{tot}}^{(\text{ss})}$ of the total disk excitation, Eq. (51). Figure 15 displays $P_{\text{tot}}^{(\text{ss})}$ versus photon energy $\hbar\omega_0$ for a 1-ps-long (spectral sharp) pulse and for different field amplitudes. Optical absorption appears at the highest exciton level placed at 4.94 eV (the doublet at about 4.5 eV is dark). The triplet positioned somewhat above 4.2 eV is represented in the absorption spectrum by a pair of lines at 4.284 eV and at 4.246 eV. Finally, we notice a

doublet above 4.0 eV. The values of $P_{\mathrm{tot}}^{(\mathrm{ss})}$ as well as unshifted peak positions indicate that we are in the linear EET regime.

The two highest peaks just described appear also in Fig. 16 where we draw $P_{\mathrm{tot}}^{(\mathrm{ss})}$ curves at a given a_p value of 5×10^5 ps V/m (upper panel) and of 10^6 ps V/m (lower panel) but for different pulse durations. For the latter value of a_p, as in the 1D case, the absorption peak below 5 eV is shifted to lower energies with increasing values of $P_{\mathrm{tot}}^{(\mathrm{ss})}$. With that, we may identify multiexciton effects as described in the case of the 6P molecular chain.

V. CONCLUSIONS

Ultrafast electronic EET in molecular systems induced by sub-picosecond laser pulses has been studied theoretically. The considerations have been restricted to the contributions of the first excited molecular electronic singlet state. However, it can be populated by different molecules simultaneously and a multiexciton state can be formed. A restricted picture of the total nonlinear response of the molecular system on laser-pulse excitation may follow, but we gained complete insight on the contribution of the first excited states. Instead of describing the temporal evolution of the multiexciton state by a direct computation of the related density matrix, we derived equations of motion for expectation values of interest. Those equations are originated by the quantum master equation governing the respective density operator. To truncate the following hierarchy of kinetic equations, a general scheme is used.

The kinetic equations were solved for a chain and a disk of *para*-sexiphenyl molecules. The spatiotemporal evolution of the molecular excitation in these 1D and 2D systems could be presented for a duration of the laser pulse excitation between 20 fs and 1 ps. Applying the longer pulse, individual exciton states may be formed. Later, if the pulse is over EET, which appears in the present description also as a dissipative process, leads to a nearly homogeneous excitation of all molecules. In contrast, the shorter pulses result in a central excitation of the *para*-sexiphenyl clusters. As an effect of nonlinear transport, we may observe Rabi-like oscillations in the excited state populations.

By drawing the steady-state value of the total excitation of the system versus the photon energy of laser pulse excitation, we may reproduce in the low excitation regime the linear absorption spectrum. When increasing the degree of excitation, the obtained low-energy shift of the absorption peaks can be considered as a multiexciton effect. Its observation in the experiment would be of particular interest. A respective additional confirmation in theory would require a more complex truncation of the hierarchy of kinetic equations compared with the one presented here. Moreover, further studies based on models which account for higher excited molecular levels are necessary to carry out a serious comparison with experiments. Both extensions would increase the numerics enormously.

ACKNOWLEDGMENTS

[1] T. Brixner, R. Hildner, J. Koehler, Ch. Lambert, and F. Wuerthner, Adv. Energy Mater. **7**, 1700236 (2017).

[2] B. M. Savoie, N. E. Jackson, L. X. Chen, T. J. Marks, and M. A. Ratner, Acc. Chem. Res. **47**, 3385 (2014).

[3] F. C. Spano and C. Silva, Annu. Rev. Phys. Chem. **65**, 477 (2014).

[4] Y. Tamai, H. Ohkita, H. Benten, and S. Ito, J. Phys. Chem. Lett. **6**, 3417 (2015).

[5] S. Reineke, M. Thomschke, B. Lüssem, and K. Leo, Rev. Mod. Phys. **85**, 1245 (2013).

[6] S. Cook, H. Liyuan, A. Furube, and R. Katoh, J. Phys. Chem. C **114**, 10962 (2010).

[7] D. Peckus, A. Devizis, D. Hertel, K. Meerholz, and V. Gulbinas, Chem. Phys. **404**, 42 (2012).

[8] S. Gòlinas, J. Kirkpatrick, I. A. Howard, K. Johnson, M. W. B. Wilson, G. Pace, R. H. Friend, and C. Silva, J. Phys. Chem. B **117**, 4649 (2013).

[9] D. C. Dai and A. P. Monkman, Phys. Rev. B **87**, 045308 (2013).

[10] S. F. Völker, A. Schmiedel, M. Holzapfel, K. Renziehausen, V. Engel, and C. Lambert, J. Phys. Chem. C **118**, 17467 (2014).

[11] F. Fennel and S. Lochbrunner, Phys. Rev. B **92**, 140301(R) (2015).

[12] K. Hader, C. Consani, T. Brixner, and V. Engel, Phys. Chem. Chem. Phys. **19**, 31989 (2017).

[13] J. Dostal, F. Fennel, F. Koch, S. Herbst, F. Wuerthner, and T. Brixner, Nat. Commun. **9**, 2466 (2018).

[14] D. Han, J. Du, T. Kobayashi, T. Miyatake, H. Tamiaki, Y. Li, and Y. Leng, J. Phys. Chem. B **119**, 12265 (2015).

[15] F. C. Spano, Phys. Rev. B **46**, 13017 (1992).

[16] G. Juzeliunas and J. Knoester, J. Chem. Phys. **112**, 2325 (2000).

[17] S. Mukamel and O. Berman, J. Chem. Phys. **119**, 12194 (2003).

[18] S. Mukamel and D. Abramavicius, Chem. Rev. **104**, 2073 (2004).

[19] H. Haug and S. W. Koch, *Quantum Theory of the Optical and Electronic Properties of Semiconductors*, 5th ed. (World Scientific, Singapore, 2009).

[20] R. Binder, S. Roemer, J. Wahl, and I. Burghardt, J. Chem. Phys. **141**, 014101 (2014).

[21] A. V. Luzanov, D. Casanova, X. Feng, and A. I. Krylov, J. Chem. Phys. **142**, 224104 (2015).

[22] X. Li, R. M. Parrish, F. Liu, S. I. L. Kokkila Schumacher, and T. J. Martinez, J. Chem. Theory Comput. **13**, 3493 (2017).

[23] V. May, J. Chem. Phys. **140**, 054103 (2014).

[24] L. Wang and V. May, Phys. Rev. B **94**, 195413 (2016).

[25] L. Wang and V. May, J. Phys. B: At. Mol. Opt. Phys. **51**, 064002 (2018).

[26] Y. Zhang and V. May, Phys. Rev. B **89**, 245441 (2014).

[27] Y. Zhang and V. May, J. Chem. Phys. **142**, 224702 (2015).

[28] L. Wang and V. May, J. Phys. B: At. Mol. Opt. Phys. **50**, 154003 (2017).

[29] L. Wang and V. May, J. Phys. Chem. C **121**, 13428 (2017).

[30] Th. Plehn, and V. May, Chem. Phys. **515**, 187 (2018).

[31] Th. Plehn, D. Ziemann, and V. May, J. Phys. Chem. Lett. **9**, 209 (2018).

[32] Th. Plehn, D. Ziemann, and V. May, Phys. Chem. Chem. Phys. **20**, 26870 (2018).

[33] Th. Plehn, D. Ziemann, and V. May, J. Phys. Chem. C **122**, 27925 (2018).

[34] E. Zojer, N. Koch, P. Puschnig, F. Meghdadi, A. Niko, R. Resel, C. Ambrosch-Draxl, M. Knupfer, J. Fink, J. L. Brédas, and G. Leising, Phys. Rev. B **61**, 16538 (2000).

[35] A. Resel, Thin Solid Films **433**, 1 (2003).

[36] M. Sparenberg, A. Zykov, P. Beyer, L. Pithan, C. Weber, Y. Garmshausen, F. Carlá, S. Hecht, S. Blumstengel, F. Henneberger, S. Kowarik, Phys. Chem. Chem. Phys. **16**, 26084 (2014).

[37] See Supplemental Material at http://link.aps.org/supplemental/ 10.1103/PhysRevB.102.075401 for details of the equations of motion.

[38] V. May and O. Kühn, *Charge and Energy Transfer Dynamics in Molecular Systems* (Wiley-VCH, Weinheim, 2011).

[39] T. Plehn, D. Ziemann, J. Megow, and V. May, J. Chem. Phys. B **119**, 7467 (2015).

[40] O. V. Prezhdo and Y. V. Pereverzev, J. Chem. Phys. **113**, 6557 (2000).